HHS Public Access

Author manuscript

Cell Rep. Author manuscript; available in PMC 2023 June 26.

Published in final edited form as:

Cell Rep. 2023 May 30; 42(5): 112426. doi:10.1016/j.celrep.2023.112426.

Transcription factor localization dynamics and DNA binding drive distinct promoter interpretations

Kieran Sweeney[1], **Megan N. McClean**[1,2,3,*]

[1]Department of Biomedical Engineering, University of Wisconsin-Madison, Madison, WI, USA

[2]University of Wisconsin Carbone Cancer Center, University of Wisconsin School of Medicine and Public Health, Madison, WI, USA

[3]Lead contact

SUMMARY

Environmental information may be encoded in the temporal dynamics of transcription factor (TF) activation and subsequently decoded by gene promoters to enact stimulus-specific gene expression programs. Previous studies of this behavior focused on the encoding and decoding of information in TF nuclear localization dynamics, yet cells control the activity of TFs in myriad ways, including by regulating their ability to bind DNA. Here, we use light-controlled mutants of the yeast TF Msn2 as a model system to investigate how promoter decoding of TF localization dynamics is affected by changes in the ability of the TF to bind DNA. We find that yeast promoters directly decode the light-controlled localization dynamics of Msn2 and that the effects of changing Msn2 affinity on that decoding behavior are highly promoter dependent, illustrating how cells could regulate TF localization dynamics and DNA binding in concert for improved control of gene expression.

In brief

Cells encode environmental information in transcription factor (TF) localization dynamics. Cells also regulate the affinity of TFs for DNA targets. Sweeney and McClean demonstrate that changing TF affinity affects the decoding of TF localization dynamics by promoters and outline how cells may exploit both modes of regulation to control expression.

Graphical abstract

*Correspondence: mmcclean@wisc.edu.

AUTHOR CONTRIBUTIONS

K.S. and M.N.M. conceived of the study. K.S. collected and analyzed data. K.S. and M.N.M interpreted results and wrote the manuscript.

DECLARATION OF INTERESTS

The authors declare no competing interests.

SUPPLEMENTAL INFORMATION

Supplemental information can be found online at https://doi.org/10.1016/j.celrep.2023.112426.

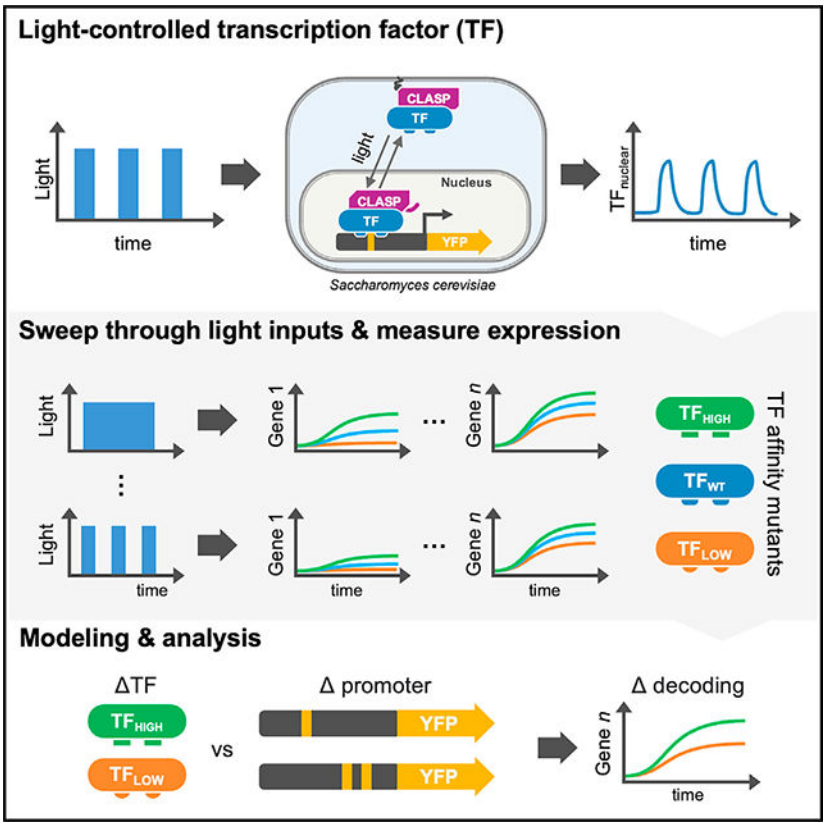

INTRODUCTION

To survive changes in their environment, cells transmit environmental information through signaling pathways to transcription factors (TFs), which bind DNA and regulate the gene expression response. Signaling pathways often exhibit a bowtie topology where multiple environmental signals converge on a single TF.[1] In these cases, how does a single TF activate the appropriate set of genes for each environmental signal? One way cells overcome this challenge is by encoding environmental information in the temporal dynamics of TF activation. For example, extracellular calcium causes the *Saccharomyces cerevisiae* TF Crz1 to translocate to the nucleus in one of two modes, continuous or pulsatile, and recent work has shown that Crz1 target genes decode its localization dynamics by preferentially activating in response to one mode over the other.[2,3] At least 10 yeast TFs and a variety of mammalian TFs exhibit similar stimulus-specific dynamics.[4–7] Beyond regulating localization, cells possess other mechanisms for modulating TF activity, each offering the opportunity to encode information. In particular, cells can regulate the ability of TFs to bind target DNA. The mammalian inflammatory response TF nuclear factor κB (NF-κB) exhibits stimulus-specific dynamics—it pulses in and out of the nucleus in response to tumor necrosis factor α (TNF-α) and undergoes sustained nuclear localization in response to bacterial lipopolysaccharides (LPSs)—but is also subject to post-translational modifications (PTMs) that regulate its ability to bind DNA.[8–12] Similarly, gamma irradiation causes short bursts of the tumor-suppressor p53, which activate DNA repair genes, but activation of

apoptotic genes may involve both sustained p53 activity and PTMs that improve DNA binding.[7,13–17]

A prime example of the bowtie topology is Msn2, a C2H2 zinc finger TF (the largest structural class of TF in eukaryotes) that regulates over 200 stress defense genes in yeast. Multiple signaling pathways (PKA, TOR, SNF) converge on Msn2, which plays a key role in the cellular response to a variety of environmental stresses.[18,19] In normal conditions, Msn2 is phosphorylated by protein kinase A (PKA) and resides primarily in the cytoplasm, but following environmental stress, Msn2 is dephosphorylated and translocates to the nucleus, where it regulates target genes by binding stress response elements (STREs) in their promoters.[20] The identity and magnitude of environmental stresses is encoded at least in part by the nuclear localization dynamics of Msn2: hyperosmotic shock causes an early, continuous pulse of nuclear localization with dose-dependent duration, while glucose starvation causes a similar early pulse that is followed by short, sporadic bursts of nuclear localization with dose-dependent frequency.[21] These stresses elicit distinct transcriptional responses, and previous work using chemical inhibition of PKA to control Msn2 localization showed that target genes decode Msn2 dynamics by exhibiting differential responses to the amplitude, duration, and frequency of Msn2 nuclear localization.[19,22,23]

We therefore use Msn2 as a model system to investigate the interplay of TF localization dynamics and binding affinity in gene induction. We partially disconnect Msn2 from upstream regulation of its localization, which we instead control with light. By combining optogenetic control of Msn2 and high-throughput microscopy, we probe the relationship between Msn2 localization dynamics and the expression of target genes. We quantify the signal decoding behavior of these genes using a computational model, which suggests that changing Msn2 affinity would have highly promoter-dependent effects on decoding behavior. We test this prediction by exploiting known mutations to the Msn2 DNA-binding domain (DBD) to create high- and low-affinity light-controlled Msn2 mutants and perform additional optogenetic experiments to quantify how such changes affect promoter decoding of Msn2 localization dynamics. By combining experiments and modeling, we identify promoter properties that allow differential responses to high- and low-affinity Msn2 mutants. We also measure the effect of tuning TF affinity on expression following natural stimuli. This study contributes a fundamental understanding of how TF affinity and localization dynamics interact with promoter properties to control gene expression.

RESULTS

Construction and optimization of a light-controlled Msn2

To bypass upstream regulation, we directly controlled the nuclear localization of Msn2 with light using CLASP (Figure 1A).[2] In this optogenetic system, Msn2 is fused at the N terminus to Zdk1, a peptide that preferentially binds a plasma membrane anchor in the dark, and at the C terminus to mScarlet and yeLANS, which features an *Avena sativa* LOV2 domain bearing a light-activated nuclear localization signal (NLS) that is largely inaccessible in the dark. When excited by blue light, Zdk1 undocks from its plasma membrane anchor, and yeLANS undergoes a conformational change that exposes its NLS to the nuclear import machinery, causing Msn2-CLASP to translocate into the nucleus, where

it can activate target genes (Figure 1B). When the blue light is turned off, Msn2-CLASP is rapidly exported from the nucleus due to a constitutive nuclear export signal (NES) within yeLANS. Since strong blue light doses may induce an Msn2-dependent stress response in yeast, [24] we also created Msn2-dCLASP (deactivated CLASP) controls lacking Zdk1 and yeLANS to verify that any observed nuclear localization was strictly due to optogenetic control.

While Msn2-CLASP exhibited rapid and reversible light-induced nuclear localization, it stochastically pulsed into the nucleus in the dark and activated target genes (Figure 1B). To disconnect Msn2 from upstream regulation of its localization, we mutated key PKA-regulated phosphosites (Figure 1C) in the NLS and NES of Msn2 that control the activity of these domains.[25] We screened the resulting Msn2-CLASP mutants for low basal nuclear localization, reduced stochastic pulsing, and the ability to localize to the nucleus and activate target genes in light (Figures S1A and S1B). We selected an Msn2 mutant (Msn2*) with four inhibitory serine-to-glutamic acid mutations in its NLS domain for further study. Msn2*-CLASP exhibited a graded response to light that plateaued near 128 a.u. and reduced stochastic pulsing and target gene activation in the dark (Figures 1D, left, and S1D–S1F). Pulsing the 128 a.u. light dose on for 2 s and off for 1 s caused only a modest decrease (5%–10%) in nuclear accumulation compared with continuous illumination, despite a 33% reduction in overall light dose (Figure 1D, right). Thus, we were able to identify the minimum light doses needed to control Msn2*-CLASP localization.

Light-sweep experiments reveal differential promoter responses to Msn2 localization dynamics

We next used Msn2*-CLASP to probe how promoters respond to defined patterns of Msn2 localization. We delivered time-varying light doses to cells and imaged the resulting pulses of Msn2* nuclear localization and reporter induction. Over these light-sweep experiments, we exposed a set of 12 reporter strains to 14 light programs that generated Msn2* localization time courses with a defined amplitude, duration, or pulsing behavior (Figures 2A and S2A). Excluding a negative control, all reporter strains featured mCitrine expressed under a promoter with at least one STRE (Figure S2B). No reporter was strongly activated by Msn2*-dCLASP following a 50 min 100% amplitude dose of blue light (Figure S2C), indicating that, without CLASP, Msn2* was not activated by the light doses used.

Our experiments showed that the signal decoding behavior of Msn2 target genes previously reported in response to modulation of PKA activity persists when Msn2 nuclear localization is controlled directly, without perturbing upstream signaling (Figure 2A).[22] For example, *HSP12* and *HXK1* were activated by every light program and exhibited a graded response to nuclear Msn2*. In contrast, *RTN2* and *SIP18* were switch-like and were not activated by short, low amplitude, and pulsatile pulses of nuclear Msn2*. To quantify these behaviors, we turned to a computational model of gene expression (Figure 2B). We modeled expression as a time-dependent function of nuclear Msn2, TF(t), in which a promoter transitions from an initial off state (P_0) to an intermediate off state (P_{off}) to an active, transcribing state (P_{on}). We pooled Msn2 localization measurements across multiple experiments, used the resulting composite signal as the model input TF(t) and fit the model for each promoter by identifying

the parameter sets that best recapitulated the measured expression time courses across all 14 light programs (fits shown in Figure S2A). Since a range of parameter sets could predict gene expression with comparable error, we ranked the parameter sets by fit and selected the best-performing ones for further analysis (Figure S3A). It should be noted that light-induced nuclear localization of Msn2* decreased over time (Figure S3B). This signal decay was not due to photobleaching (Figure S3C) and appeared to affect target gene induction, as our localization measurements consistently provided better model fits than simulated Msn2 time courses without decay (Figure S3D). The cause of the signal decay is unknown, though previous studies suggest it could be due to increased degradation of Msn2 in the nucleus or inactivation of the LOV2 domain.[26–29]

Gene expression model reveals promoter groups with distinct signal decoding behaviors

Based on previous studies,[22,23] we used the model to calculate amplitude thresholds and activation timescales, which, respectively, describe the amplitude and duration of a square pulse of nuclear Msn2 needed to attain half-maximum promoter activation (Figures 2C and S3E). The amplitude threshold and activation timescale were linearly related ($R^2 = 0.69$): promoters with low amplitude thresholds (like *HXK1*, *HSP12*, *SIP18 A4*, and *DDR2*) had short activation timescales, while promoters with high amplitude thresholds (like *RNT2*, *TKL2*, *SIP18*, and *ALD3*) had long activation timescales. Both the amplitude threshold and activation timescale were inversely related to the predicted value of K^n for each promoter. K^n captures the half-maximum point (K) and slope (n) of the curve relating nuclear Msn2 levels to the rate of transition from P_0 to P_{off} and is inversely related to the affinity between the promoter and Msn2 (Figure S3F). In turn, K^n was inversely related to the number of STREs for most promoters (Figure S3G). The top parameter sets for promoters with high amplitude thresholds and long activation timescales, like *RTN2*, tended to have high values of K^n, implying a low affinity for Msn2, while promoters with low amplitude thresholds and short activation timescales, like *HSP12*, were enriched for low values of K^n, implying a high affinity for Msn2 (Figure 2D, top). We therefore quantified the affinity of each promoter for Msn2 as the mean value of $\log_{10}(K^n)$ for the top 0.1% of parameter sets (Figure 2D, bottom).

Taken together, the amplitude thresholds, activation timescales, and predicted values of K^n revealed three groups of promoters: high, mid, and low sensitivity (highlighted in Figures 2C and 2D). The high-sensitivity promoters had low predicted values of K^n, low amplitude thresholds, and short activation timescales, reflecting an ability to respond rapidly to small amounts of nuclear Msn2. In contrast, the low-sensitivity promoters had high predicted values of K^n, high amplitude thresholds, and long activation timescales, reflecting their tendency to filter out short, low-amplitude doses of nuclear Msn2. The mid-sensitivity promoters were characterized by intermediate predicted values of K^n and amplitude thresholds but had activation timescales that overlapped both the high- and low-sensitivity groups. These results imply that the signal decoding behavior of the promoters is at least partly set by their affinity for Msn2.

Gene expression model predicts that slow, low-affinity promoters are most strongly affected by changes in TF binding affinity

Previous work showed that increasing or decreasing the DNA binding affinity of Msn2, respectively, increases or decreases the expression of target genes at steady state.[30] However, it was unclear how such changes would affect promoter decoding of Msn2 dynamics. We performed a sensitivity analysis of the gene expression model shown in Figure 2B by simulating the expression of hypothetical promoters with varying kinetic parameters (k_1, d_1, k_2, d_2, and k_3) and baseline affinities to a TF (K), which predicted that changes in baseline affinity (K) would strongly affect genes with slow activation kinetics (low k_1 or k_2) or fast deactivation kinetics (high d_1 or d_2) (Figure 3A). We next asked how would the expression of promoters with a high or low baseline affinity to a TF (low or high K, respectively) be affected by additional, relatively small shifts in affinity caused by PTMs modulating the ability of the TF to bind target DNA? To model the response of hypothetical promoters with widely varying baseline affinities to an additional 2-fold increase or decrease in the affinity of the TF for DNA, we simulated the expression of each promoter while scaling K by $\alpha = 0.5$ or $\alpha = 2$, respectively (as depicted in the modified gene expression model of Figure 3B, top). For simplicity, we fixed the Hill coefficient (n) at a value of one. The predicted expression of promoters with a low baseline affinity to the TF (high K)was strongly affected by changes in TF affinity for target DNA, whereas promoters with a high baseline affinity (low K) were only weakly affected (Figure 3B, bottom). Overall, our simulations suggested that promoters requiring slow nucleosome remodeling steps (slow activation kinetics) or promoters with few, weak, or occluded TF binding sites (low baseline affinity) would be most strongly affected by changes in TF affinity for DNA, while promoters with fast activation kinetics or many open TF binding sites (high baseline affinity)would be less sensitive to such changes.

Having identified potential mechanisms by which modulating the ability of a TF to bind DNA would differentially affect target gene expression, we moved from hypothetical promoters to ask how a 2-fold increase or decrease in the ability of Msn2 to bind DNA would affect the signal decoding behavior of our Msn2 reporter genes. As before, we simulated the response of each reporter to a pulse of nuclear Msn2 while scaling K by $\alpha = 0.5$ or 2, respectively. The predicted effects of changing Msn2 affinity for DNA were highly promoter dependent (Figure 3C). Changes to Msn2 affinity weakly affected the predicted expression of high-sensitivity genes like *HSP12*, and there was little expression gained for further increases in TF affinity. In contrast, changes to Msn2 affinity strongly affected the predicted expression of low-sensitivity genes like *RTN2*. In fact, the model predicted that increasing Msn2 affinity would effectively allow the induction of *RTN2* by pulsatile doses of nuclear Msn2. As discussed below, the gene expression trends predicted by the model were confirmed experimentally (Figure 3D).

Thus far, we had only examined how changes in Msn2 affinity affected expression following a single pulse of nuclear localization. To investigate if changes in Msn2 affinity for DNA conferred an advantage in activating genes in certain localization conditions, particularly pulsed versus sustained conditions, we calculated the maximum expression of the target genes for a range of nuclear localization patterns while scaling K as described above. As

expected, increasing the affinity of Msn2 for DNA generally increased maximal expression, and long-duration, high-amplitude pulses of nuclear Msn2 induced stronger expression than low-amplitude, short-duration, or pulsed doses (Figure 3E, top). However, normalizing the predicted expression of each reporter to its expression for Msn2* ($\alpha = 1$) showed that changing Msn2 affinity did not strongly affect the relative expression between localization conditions (Figure 3E, bottom). That is, the model predicted that changing the Msn2 affinity does not confer an advantage in activating genes following pulsed doses of Msn2 localization over sustained doses. Rather, as confirmed below, the relative ability to respond to pulsed versus continuous doses of TF localization is intrinsic to the promoter.

Light-sweep experiments reveal divergent responses to Msn2 affinity changes between high- and low-sensitivity promoters

To test the model's predictions, we exploited known mutations to the DBD of Msn2 (Figure S4A). We created Msn2(A)*, which has a high predicted affinity to its targets and is transcriptionally hyperactive, and Msn2(T)*, which has a low predicted affinity and reduced transcriptional activity (Figures S4B and S4C).[30–32] With CLASP, the expression levels and localization behavior of Msn2(A)* and Msn2(T)* were similar to Msn2* (Figures S2A, S4D, and S4E), and reporter induction by these mutants following a single pulse of blue light broadly agreed with our model's predictions (compare Figures 3C and 3D). These expression differences were confirmed at the mRNA level using fluorescence *in situ* hybridization (FISH; Figure S4F). To characterize how changes in Msn2 affinity affect the signal decoding behavior of its targets, we performed additional light-sweep experiments with Msn2(A)* and Msn2(T)* (Figure 4).

We first considered the response of the target promoters to single pulses of each Msn2 mutant with varying amplitudes or durations (shown for the low-sensitivity promoter *RTN2* and the high-sensitivity promoter *HSP12* in Figure 5A). Overall, increasing Msn2 affinity increased reporter expression and reduced the amplitude threshold and activation timescale of the promoters such that lower pulse amplitudes and durations were needed to achieve a given level of activation (Figure S4G), though as predicted, the magnitude of these effects was highly promoter dependent. For the low-sensitivity promoters, there were generally large expression differences between Msn2 mutants across most localization conditions. For example, single pulses of Msn2(A)* with increasing amplitudes or durations allowed the robust, tunable induction of *RTN2*—to levels 3.7-fold higher than Msn2* at the maximum light dose—while Msn2(T)* failed to activate *RTN2* in most cells across all conditions (Figure 5A, top). For the low-sensitivity promoters, the relationship between the area under the curve (AUC) of Msn2 nuclear localization and expression was nonlinear: these promoters filtered out short-duration or low-amplitude pulses of nuclear localization and were especially dependent on the nuclear concentration (amplitude) of Msn2. For example, maximum *RTN2* expression for a 30 min 100% amplitude pulse of Msn2(A)* (AUC = 26.8) was 1.7-fold higher than for a 50 min 75% amplitude pulse (AUC = 28.2; compare circled points in Figure 5A) despite both pulses having a nearly identical AUC. In contrast, single pulses of all three Msn2 mutants allowed the robust, graded activation of high-sensitivity promoters like *HSP12*, and expression differences between the mutants were typically small (Figure 5A, bottom). As with *HSP12*, whether increasing pulse amplitude or pulse

duration, expression of the high-sensitivity promoters increased linearly with the AUC of Msn2 nuclear localization, though in some cases, it approached saturation at high pulse amplitudes. There was no high-sensitivity promoter where expression for Msn2(A)* was significantly higher than for Msn2*, suggesting that there was little expression gained for further increases in Msn2 affinity for such genes. In fact, doing so may have a cost, as expression of *HXK1* and *DDR2* was weakly but consistently lower for Msn2(A)* versus Msn2* (see Figure S2A).

Relative ability to respond to pulsed versus continuous doses of nuclear Msn2 is primarily set by the promoter

Having analyzed the response of our target genes to single pulses of each Msn2 mutant, we next considered their response to pulsatile doses of nuclear localization. Our gene expression model predicted that increasing Msn2 affinity would generally increase the absolute expression of our target genes for pulsatile doses of nuclear localization and effectively allow the induction of low-sensitivity genes in pulsatile conditions. Indeed, our light-sweep experiments confirmed that Msn2(A)* could activate the low-sensitivity promoters in pulsatile localization conditions where Msn2* and especially Msn2(T)* did not (see conditions 10–14 in Figure 4). In the case of *RTN2*, expression for six 5 min pulses of Msn2(A)* was 1.9-fold higher than for a comparable 30 min continuous pulses of Msn2* (see circled points in Figure 5B, discussed below).

However, our gene expression model also predicted that relative differences in target gene expression between Msn2 mutants should be stable across conditions—that is, changing Msn2 affinity should not affect the relative ability of a promoter to respond to pulsed versus continuous doses of nuclear localization (see Figure 3E). To test this, our light-sweep experiments included several pairs of conditions with comparable pulsed or continuous doses of each Msn2 mutant (shown for *RNT2* and *HSP12* in Figure 5B). *HSP12* responded to pulsed (triangular points) and continuous (circular points) doses of nuclear localization almost equally well. In contrast, for both Msn2* and Msn2(A)*, induction of *RTN2* was much stronger for continuous doses of nuclear localization than pulsed doses, while Msn2(T)* failed to induce *RTN2* in most cells in any condition. The measurements also demonstrated that increasing the number of pulses of nuclear Msn2 allowed the graded induction of either promoter. To quantify the relative ability of our target genes to respond to pulsed versus continuous doses of each Msn2 mutant, we calculated slope ratios by fitting lines to the measurements and dividing the slope of the pulsed line (dashed) by the slope of the continuous line (solid).[2] A slope ratio less than one indicates stronger promoter induction by a continuous dose of nuclear Msn2 than a pulsatile dose, while a slope ratio greater than one indicates the opposite.

Overall, there were large differences in slope ratio between promoters: the high-sensitivity promoters were strongly induced by pulsatile doses of nuclear Msn2 and, accordingly, had high slope ratios, while the low-sensitivity promoters were poorly activated by pulsatile doses of Msn2 and had low slope ratios (Figure 5C). On the other hand, differences in slope ratio between Msn2 mutants for a given promoter were comparatively small and possibly a consequence of signal decay, which should disproportionally affect the longer pulsatile light

doses (Figure S3B) by causing nuclear Msn2 levels to drop below the elevated amplitude thresholds typically associated with a decrease in Msn2 affinity (Figure S4G). To compare the effects of increasing promoter affinity by adding TF binding sites versus increasing TF affinity for target DNA, we analyzed the expression of *SIP18* and its mutants, *SIP18 A4* and *SIP18 D6* (Figures 5C and S5A). *SIP18* was weakly expressed and had a low slope ratio; adding a cluster of STREs distal to its TATA box (*SIP18 D6*) moderately increased its expression but not its slope ratio, while adding a cluster of STREs proximal to its TATA box (*SIP18 A4*) increased both its expression and slope ratio. In contrast, increasing Msn2 affinity increased the expression of these promoters but not their slope ratios. Taken together, these observations indicate that the relative ability to respond to pulsed versus continuous doses of Msn2 is primarily set by promoter properties such as the location and availability of TF binding sites rather than by the TF.

Decreasing Msn2 affinity increases gene expression noise

Having examined how our target genes responded to the localization dynamics of each Msn2 mutant at a population level, we next considered their responses at a single-cell level. We quantified cell-to-cell expression variability, or noise, in the light-sweep experiments (Figure S5B). As expected, there was a negative correlation between gene expression strength and noise ($R^2 = 0.81$) such that low-sensitivity promoters were much noisier than high-sensitivity promoters (Figure S5C). Similarly, the decrease in gene expression typically caused by decreasing Msn2 affinity was accompanied by an increase in noise. Msn2 localization dynamics also affected expression noise, which was higher for pulsed doses of nuclear localization than continuous doses. These effects can be seen by comparing single-cell expression measurements of *HSP12* and *RTN2* (Figure 5D). *RTN2* was (weakly) expressed in just 13.8% of cells following a pulsatile dose of Msn2(T)* versus 39% of cells for a continuous dose of Msn2(T)*. In contrast, a pulsatile dose of Msn2(A)* moderately activated *RTN2*, and a continuous dose of Msn2(A)* maximized *RTN2* expression. Meanwhile, either pulsed or continuous doses of Msn2(T)* or Msn2(A)* were sufficient to robustly activate *HSP12* with comparatively low expression noise (Figure S5B). As explored further in the discussion, these measurements hint at how the concerted regulation of TF localization dynamics and affinity may facilitate tighter control of expression.

Changing Msn2 affinity alters a cell's ability to discriminate between stresses

Msn2(A)* induced low-sensitivity promoters like *RTN2* and *TKL2* following pulsatile doses of nuclear localization where Msn2* and Msn2(T)* did not. We therefore predicted that Msn2(A)* may similarly be better at inducing these genes following glucose starvation, which naturally causes sporadic pulses of Msn2 nuclear translocation, versus hyperosmotic shock, which naturally causes an early, sustained pulse of nuclear localization with a dose-dependent duration.[21] To test this, we measured reporter expression following glucose starvation and hyperosmotic shock for Msn2, Msn2(A), and Msn2(T)—all without CLASP or any mutations outside their DBDs (Figures 6 and S6A). Overall, expression of most promoters was highest for Msn2(A) and lowest for Msn2(T). While all three Msn2 mutants activated the low-sensitivity genes *RTN2* and *TKL2* in response to hyperosmotic shock, only Msn2(A) activated them in response to glucose starvation. In essence, these genes lost their ability to discriminate between the stresses when the affinity of Msn2 for target DNA

was increased. This was not due to differences in localization behavior, as Msn2(A) and Msn2 had similar localization dynamics (Figure S6B). Excluding *DDR2*, which was most strongly induced by Msn2, there were few significant differences in the expression of the high-sensitivity promoters between Msn2(A) and Msn2 (see Figure S6A), which agrees with our model's predictions that, at a point, there are few expression gains for further increases in TF affinity.

DISCUSSION

Previous work by Hansen and O'Shea showed that Msn2 target genes decode the patterns of Msn2 localization generated by modulating PKA activity. However, other proteins downstream of PKA also affect expression—including the TFs Hsf1, Sok2, and Dot6 and components of the mediator complex—and could contribute to signal decoding by Msn2 target genes.[33–36] Our measurements show that signal decoding by Msn2 targets persists when Msn2* localization is controlled directly. Consequently, the promoters act as filters of Msn2 dynamics: low-sensitivity genes filter out low-amplitude, short-duration, and pulsatile doses of nuclear Msn2, while high-sensitivity genes are readily induced and effectively integrate the nuclear Msn2 signal. While our results are broadly consistent with those of Hansen and O'Shea, some promoters behaved differently than expected: *DCS2* and *RTN2* were less readily activated, and *SIP18 D6*, which was previously reported to have a low amplitude threshold and high activation timescale, had intermediate values of both (Figure 2C). Accordingly, we observed no decoupling of amplitude threshold and activation timescale, which were linearly related for all promoters measured. Such differences may be due to differences in methodology. Beyond employing optogenetic control of Msn2 rather chemical control of PKA, we also used fluorescent reporters integrated at the URA3 locus rather than at the open reading frame (ORF) of each reporter gene.

Our light-sweep experiments systematically probed how changes to the affinity of Msn2 for target DNA affected promoter decoding of its nuclear localization dynamics (Figure 4). Increasing Msn2 affinity increased the expression of its target genes, making them more responsive to shorter, weaker, and pulsatile doses of nuclear localization. These effects were much stronger for low-sensitivity genes than high-sensitivity genes. In fact, some low-sensitivity genes lost the ability to discriminate between natural stresses when Msn2 affinity was increased (Figure 6), which is consistent with suggestions that the ability of TFs to bind DNA is tuned for function and that high TF binding affinities are not necessarily optimal.[37,38] A sensitivity analysis of our expression model indicated that—beyond baseline promoter affinity—slow promoter activation kinetics or fast deactivation kinetics could also cause divergent responses to TF mutants with a high or low affinity to their binding site. Moreover, while increasing Msn2 affinity and adding Msn2 binding sites to the *SIP18* promoter both increased gene expression, only changes to the *SIP18* promoter itself affected its relative ability to respond to pulsed versus continuous doses of nuclear localization. This is consistent with a proposal that *SIP18 A4* is more responsive to short or pulsed bursts of nuclear Msn2 than *SIP18 D6* because it facilitates Msn2 binding and subsequent chromatin remodeling at the TATA box.[23]

Expression increases due to increased Msn2 affinity were typically accompanied by a decrease in noise (Figure S5C). Noisy expression can be beneficial as a source of phenotypic diversity between cells but limits the information transduction capacity of genes. Hansen and O'Shea previously identified a trade-off between noise and control of gene expression: low-sensitivity promoters filter out noisy TF activity but respond to real signals with high levels of expression noise, while high-sensitivity promoters have low expression noise but are readily induced by noisy bursts of TF activity.[22,39] Various strategies have been proposed for overcoming the effects of noise in decoding TF dynamics: integrating the response of multiple genes to overcome the noisy expression of individual genes, recruiting chromatin regulators to fine-tune the information capacity of a given gene, and coordinated gene regulation by multiple TFs.[40–42] Our results point to another potential mechanism for selectively activating genes: concerted regulation of TF localization dynamics and DNA binding, which could exploit promoter-dependent differences in responsiveness to both modes of regulating TF activity. We could tune the expression of high-sensitivity promoters while minimally inducing low-sensitivity promoters using doses of Msn2(T)* with varying amplitudes, durations, or pulse numbers (Figure 5A), while robust, graded activation of the low-sensitivity promoters was possible only with Msn2(A)*. Perhaps more subtly, control of both TF affinity and localization could tune the expression of low-sensitivity genes while maintaining the robust expression of high-sensitivity genes (Figure 7). Thus, a TF capable of transitioning between high- and low-affinity DNA-binding modes and exhibiting stimulus-specific localization dynamics could facilitate tightly controlled, graded activation of specific sets of genes in different conditions. Such regulation may be beneficial to avoid activating resource-intensive or terminal cell fate genes when responding to mild stresses. Future studies are needed to determine if cells employ such strategies to coordinate stress-specific gene expression responses via TFs (like p53 and NF-κB), whose localization dynamics and DNA-binding affinity are both subject to regulation.

Mechanistically, what drives the different behaviors of the high- and low-sensitivity promoters? Our gene expression model identified the affinity between a promoter and a TF as a key factor. Indeed, no low-sensitivity promoter had more than two STREs within 500 bp of its ORF, while no high-sensitivity promoter had fewer than four STREs in the same region (Figure S2B), which is consistent with observations that increasing the number of TF binding sites in a promoter generally increases its affinity for the TF and maximum expression.[43,44] Differences in nucleosome occupancy between the high- and low-sensitivity promoters may also drive differences in their behavior and manifest as differences in affinity by restricting access to STREs. Induction of the low-sensitivity promoter *SIP18* involves a slow chromatin remodeling step before initiating transcription, as do mammalian genes that require sustained NF-κB activity.[22,23,45] Likewise, Crz1 target promoters with low slope ratios are typified by a slow transition from an initial off state (P_0) to an intermediate off state (P_{off}) that is associated with high initial nucleosome occupancy at the promoter.[2] Our low-sensitivity reporters had both long activation timescales and low slope ratios (Figures 2C and 5C) and were enriched for low predicted values of k_1 and high predicted values of K^n—all consistent with a slow transition step involving chromatin remodeling (Figure S3A). The general inability of Msn2(T)* to activate these promoters hints that it may be poor at initiating chromatin remodeling. Activation of latent enhancers in murine macrophages

by NF-κB requires continuous NF-κB activity to disrupt histone-DNA interactions, and competition with nucleosomes has also been implicated in the activation of yeast genes by Rap1.[46,47] In fact, the affinity of exposed Pho4 binding sites in the promoters of yeast phosphate response genes determines the level of phosphate starvation—and thus nuclear Pho4—needed to nucleate chromatin remodeling and activate gene expression.[43] Further studies are needed to determine if the reduced DNA-binding ability of Msn2(T)* similarly limits its ability to compete with nucleosomes and initiate chromatin remodeling events.

Limitations of the study

Previous studies have shown that TF activity gates transcriptional bursting and that the resulting burst statistics affect integrated gene expression,[48] which we measured indirectly via a fluorescent reporter protein. Based on our results, we would expect high-sensitivity genes to have higher burst frequencies and lower expression noise than low-sensitivity genes. Future studies using mRNA-level reporters could explore in more detail such transcriptional differences for high- and low-sensitivity genes or high- and low-affinity TF mutants.[49]

STAR★METHODS

RESOURCE AVAILABILITY

Lead contact—Further information and requests for resources and reagents should be directed to and will be fulfilled by the lead contact, Megan N. McClean (mmcclean@wisc.edu).

Materials availability—Yeast strains and plasmids generated for this study are available by request to the lead contact.

Data and code availability

- The timelapse microscopy images reported in this study cannot be deposited in a public repository because of file size constraints. To request access, contact the Lead Author. Single-cell fluorescence measurements extracted from the images and flow cytometry measurements for yeast subjected to natural stimuli have been deposited at Mendeley Data and are publicly available as of the date of publication. DOIs are listed in the key resources table.
- All original code has been deposited at Zenodo and is publicly available as of the date of publication. DOIs are listed in the key resources table.
- Any additional information required to reanalyze the data reported in this paper is available from lead contact upon request.

EXPERIMENTAL MODEL AND SUBJECT DETAILS

Strain and plasmid construction—The *Saccharomyces cerevisiae* strains used in this study were constructed from a base strain in the S288C background (MAT alpha his3D1 leu2D0 lys2D0 MET15 ura3D0). To identify the nucleus, the nuclear protein Nhp6a was tagged with the infrared fluorescent protein iRFP via URA3 pop-out. Briefly, this entailed

tagging the C-terminal of Nhp6a using a caURA3 selective marker that was subsequently "popped out" by counterselection with 5-Fluoroorotic acid (5FOA) and a repair DNA template coding for iRFP. To avoid interference with the Msn2-CLASP mutants, the native copy of Msn2 and its paralog Msn4 were deleted in the base strain, also by URA3 pop-out.

Reporter strains were subsequently constructed from the base strain. Reporters were selected as follows: *HXK1, DCS2, SIP18, SIP18 A4, SIP18 D6, DDR2, TKL2, ALD3,* and *RTN2* were selected based on previous studies of the relationship between Msn2 nuclear localization and gene expression,[22,23] *CTT1* was selected because it was used to study Msn2(S686A) activity,[32] and *HSP12* was selected because it was used to test Msn2-CLASP performance.[2] We also constructed a no reporter control strain featuring GFP expressed under a bacterial promoter that is silent in yeast (*glpT*). To create each reporter strain, the region 1000 bp upstream of the open reading frame of each reporter gene was amplified by PCR and inserted by Gibson assembly into an integrating plasmid such that it drove the expression of mCitrine. The reporter plasmids were screened by sequencing, linearized by digestion with NotI-HF, and integrated into the LEU2 locus of the base strain using the LiAc/ssDNA/PEG yeast transformation method.[54,55]

The Msn2 mutants were made using overlap PCR to mix and match, in a modular fashion, Msn2 domains with phosphomimetic mutations, which were generated by PCR or purchased as gBlocks from IDT. The Msn2 mutants were then added by Gibson assembly to a CLASP plasmid without a cargo protein (Addgene #133086), which was generously provided by Lindsey Osimiri and Hana El-Samad. Similarly, an equivalent dCLASP plasmid, lacking Zdk1 and yeLANS, was created for each Msn2 mutant by Gibson assembly. The Msn2-CLASP and Msn2-dCLASP plasmids were screened by sequencing and integrated into the URA3 locus of the reporter strains as described above. The resulting transformants had inconsistent levels of mScarlet, suggesting that Msn2-CLASP sometimes integrated more than once, likely because regions of self-homology in the Msn2-CLASP plasmids were undergoing homologous recombination when transformed into yeast. Accordingly, we screened all transformants by flow cytometry for consistent, low mScarlet levels prior to use in the light sweep experiments. Strains and plasmids used for the light sweep experiments and the flow cytometry experiments of Figure 6 are listed in Tables S1 and S2, respectively.

Plasmid construction was done using DH5alpa competent cells. Yeast transformations were done using SC agar plates with appropriate auxotrophic or drug selection. After screening, yeast were frozen down and grown out on YPD plates for subsequent use in experiments. For all flow cytometry and microscopy experiments, yeast were grown in LFM created from YNB without ammonium sulfate, without folic acid, without riboflavin (MP Biomedical 4030–512).[56] For practical reasons, strain construction was done under room lights, but all strains were incubated and stored in the dark.

METHOD DETAILS

Blue light delivery—Blue light stimulation was performed using an optoPlate.[52] The optoPlate was modified with custom 3D printed adaptors to allow mounting upside-down over a 96 well plate on an inverted fluorescence microscope and custom software to allow 1) communication with the microscope, 2) programming of the optoPlate with a plate map

recording the light pattern for each well, and 3) calibration of the LEDs.[53] After calibration, the relationship between LED amplitude (0–255 AU) and irradiance was quantified (Figure S1C).

Light sweep experiments conditions—In each light sweep experiment, reporter induction was measured for two Msn2-CLASP mutants, each subjected to 14 light programs with blue light pulses spanning a range of amplitudes, durations, and oscillatory patterns (depicted in Figure S2A, top panel). Light programs 1–5 featured 50 min pulses of blue light with amplitudes of 0, 20, 45, 85, and 128 AU. Light programs 6–9 featured pulses of 128 AU blue light with durations of 10, 20, 30, and 40 min. Light programs 10–12 featured 2, 6, and 10 5 min pulses of 128 AU blue light with interpulse durations of 5 min. Light programs 13 and 14 featured 6 5 min pulses of 128 AU blue light separated by 10 and 15 min, respectively. Each light sweep experiment also included a full light (50 min 128 AU) dCLASP control with the appropriate Msn2 mutants (light program 15) and batch controls in which *HXK1* expression was measured for Msn2*-CLASP with both a 50 min 128 AU light dose and no light (light program 16). All light programs included 2 s off, 1 s on pulse width modulation of the light dose. In total, 32 wells were imaged per light sweep experiment. For a given reporter strain and pair of Msn2-CLASP mutants, three light sweep experiments were performed, one for each of three biological replicates.

The cultures used for each light sweep experiment were grown over multiple days so that they reached mid-log phase by the morning of each experiment (day 0). Briefly, on the evening of day −2, single colonies were picked into 100 μL LFM in 96 well plate and grown at 30°C overnight. On the evening of day −1, the resulting saturated cultures were serial diluted 1:7000 into 3 mL LFM in test tubes and grown on a roller drum at 30°C for 15 h. By the morning of day 0, the diluted cultures reached mid-log phase and were used for one of three rounds of light sweep experiments throughout the day. Cultures for the first round of experiments were used immediately, while those for the second and third rounds were, respectively, diluted back 1:5 into 3 mL LFM and grown at 30°C for 3–4 h or diluted 1:30 into 3 mL LFM and grown for 7–8 h. All day 0 steps were done with 30°C LFM and in dark.

Light sweep experiments microscopy—Light sweep experiments were done in optical 96 well plates (CellVis P96–1.5H-N) pretreated with concanavalin A (MP Biomedicals) to allow cells to adhere to the plate bottom and immersion oil to facilitate the use of an oil immersion microscope objective. Briefly, 30 μL of 2 mg/mL concanavalin A was added to each well used, incubated at room temperature for 15 min, and removed. The bottom of the 96 well plate was then coated with immersion oil (Olympus, Type F). Cultures to be imaged were diluted to OD600 = 0.125–0.150 in LFM and plated in an optical 96 well plate, which was then loaded onto the stage of an inverted fluorescence microscope (Nikon TiE) that was kept dark and at 30°C by an incubating enclosure. The cells were allowed to settle and adhere to the plate bottom for 15 min, at which point the media was removed, the cells were washed three times with LFM, and fresh LFM was added. The cells were then allowed to equilibrate for at least 10 min, during which time an optoPlate was mounted upside-down over the 96 well plate, connected to the microscope computer via USB, and configured to deliver the appropriate light dose to each well.

For each light sweep experiment, each well was imaged every 2.5 min for 160 min using a Nikon TiE inverted microscope equipped with a 60x oil immersion objective, an automated stage, and a CCD camera. The microscope was controlled by NIS-Elements and acquired 3 images for each of 32 wells per time point: an iRFP image of the nuclear marker (400 ms, Nikon Intensilight lamp with 540/45× 720/60m Cy5.5 filter cube, 1.5x gain, ND8, extended NIR mode), an mScarlet image of the Msn2-CLASP mutant (400 ms, Nikon Intensilight lamp with 560/40× 630/75m mCherry filter, ND8, 1.5x gain), and a YFP image of the mCitrine reporter (75 ms, Nikon Intensilight lamp with 510/20× 545/30m rsYFP (red-shifted YFP) filter cube, ND8, 1.5x gain). Focus was maintained using the Nikon Perfect Focus System (PFS). The rsYFP (red-shifted YFP) cube and 75 ms exposure at ND8 were selected to limit light-induced localization of Msn2-CLASP when imaging. Occasionally, the PFS lost focus due to changes in height over the large plate area being imaged or the optoPlate shifting slightly; in these cases, focus was re-established using custom NIS-Elements scripts. When imaging commenced, NIS-Elements instructed the optoPlate to initiate, allowing the timelapse microscopy and light program to operate in sync. Each light program included a 10 min delay before the blue LEDs were activated such that basal fluorescence could be measured. The microscope instructed the optoPlate to turn off the LEDs in each well as it was imaged.

Over the course of the light sweep experiments, over 2300.ND2 timelapse images were acquired, one for each of 32 wells per experiment. To automate the handling of this large amount of image data, the strain loaded in each well and the light program to which it was subjected were recorded in a spreadsheet (a “plate map”) that was saved with each set of images. Using custom MATLAB scripts, the plate map was subsequently used to automatically label the ND2 images and the single cell fluorescence measurements extracted from them.

Flow cytometry experiments with natural stress—As with the light sweep experiments, stains used for flow cytometry experiments were grown over the course of three days. On the evening of day −2, four colonies of each strain were picked into 100 μL of LFM in a 96 well plate and incubated at 30°C overnight. On the evening of day −1, the resulting saturated cultures were diluted 1:1600 into 200 μL LFM in a new 96 well plate and incubated at 30°C for 14 h. On the morning of day 0, 20 μL of each culture was aliquoted into 8 plates containing 140 μL 30°C LFM and incubated 4 h at 30°C. The cultures were pelleted by centrifuging for 5 min at 3200 rpm and then forcefully tipping out the supernatant. The pellets were resuspended in control media (30°C LFM), hyperosmotic shock media (30°C LFM with 0.5, 0,25,0.125, or 0.0625 M NaCl), or glucose deficient media (30°C LFM with 0.5, 0.1, or 0.01% glucose) and grown for 2 h at 30°C. To arrest translation, 40 μL of 0.5 μg/mL cycloheximide was added to each culture and allowed to incubate at 30°C for 30 min, at which point 20 μL of each arrested culture was added to 140 μL 4°C PBS 0.1% tween in a 384 well plate. The cells were then measured with an Attune NxT flow cytometer equipped with an autosampler: mScarlet was measured with 561 nm excitation light and a 585/16 nm filter and mCitrine was measured with a 488 nm excitation light and 590/40 nm filter. Rainbow beads were used to ensure day-to-day consistency in intensity measurements.

Gene expression model—The gene expression model (depicted in Figure 2B) features three promoter states and represents the production of mature YFP (mYFP) as a function of Msn2 with the following ordinary differential equations:

$$\frac{dP_{unbound}}{dt} = d_1 P_{bound} - \frac{k_1 Msn2(t)^n}{K^n + Msn2(t)^n} P_{unbound}$$

$$\frac{dP_{bound}}{dt} = \frac{k_1 Msn2(t)^n}{K^n + Msn2(t)^n} P_{unbound} + d_2 P_{active} - d_1 P_{bound} - k_2 Msn2(t) P_{bound}$$

$$\frac{dP_{active}}{dt} = k_2 Msn2(t) P_{bound} - d_2 P_{active}$$

$$\frac{dmRNA}{dt} = k_3 P_{active} - d_3 mRNA$$

$$\frac{dYFP}{dt} = k_4 mRNA - d_4 YFP - k_5 YFP$$

$$\frac{dmYFP}{dt} = k_5 YFP - d_4 mYFP$$

This three-state model of promoter activation was chosen based on previous reports that a transition between two off states (P_0 and P_{off}) captures the behavior of slow promoters like *SIP18* by representing chromatin remodeling steps needed for activation.[2,22,45] To capture the switch-like activation of some promoters, we modeled this transition with a Hill function, where K and n capture the half-maximum point and slope of the curve relating nuclear Msn2 concentration to the rate of promoter transition. K^n is related to the binding affinity between the promoter and Msn2, which is determined by the sequence, number, and location of Msn2 binding sites in the promoter as well as other factors like competition and nucleosome occupancy.[23,30,43,44]

To parameterize the models, pooled Msn2 localization measurements (shown in Figure S3B) were interpolated and used as the input TF(t) and the predicted YFP level (mYFP) was fit to the time-resolved localization measurements for reporter and Msn2 DBD mutant across all light programs. More specifically, we calculated expression for each light program for 100,000 parameter sets obtained by Latin hypercube sampling in which the promoter-specific parameters were allowed to vary over the following ranges: k_1, k_2, and k_3 from 10^{-3} – 10^2, K from 1 – 10^4, n from 0.5–4, and d_2 from 10^{-4} – 10^2. Global parameter values $d_4 = 0.08$, $k_4 = 15$, $d_4 = 0.001$, and $k_5 = 0.06$ were taken from the literature.[22] We then ranked

the parameter sets by how well they minimized the residual sum of squares error between the predicted and measured expression across all light programs.

Promoter categorization—Amplitude thresholds and activation timescales were calculated using the gene expression model and respectively denote the amplitude and duration of nuclear Msn2* needed to reach half the maximum promoter activity (k_3P_{on}) attained by a 50 min 100% amplitude ideal pulse of nuclear Msn2* (as shown in Figure S3E). Promoter categories were obtained by k-means clustering of the amplitude thresholds, activation timescales, and predicted values of K^n for Msn2*-CLASP using MATLAB's *kmeans* function.

Western blots—Strains were grown at 30°C in YPD to reach OD600 = 0.4–0.6 and harvested by centrifugation. Cell extracts were prepared by resuspending the pellets in cold buffer A (50 mM HEPES, 0.4 M $(NH_4)_2SO_4$, 1mM EDTA, 5% glycerol) with protease inhibitors and bead beating at 4°C for 2 min four times, with 2 min breaks on ice between bead beating rounds. Lysate was removed from beads and Triton X- was added to a final concentration of 1% before centrifuging for 30 min at 20,000 g and 4°C. Total protein (the supernatant) was denatured in 1X SDS running buffer (1X NuPage LDS sample buffer, 10% β-mercaptoethanol) with protease inhibitors by heating at 95°C for 10 min and then chilled on ice for 2 min. Subsequently, 30 μL of the denatured protein extract was separated by SDS-PAGE using an Invitrogen Bolt 4–12% Bis-Tris acrylamide gel and transferred onto a 0.2 μm nitrocellulose membrane. Immunoblots were developed using the Pierce Supersignal Femto Kit and imaged with a Bio-Rad ChemiDoc XRS+ system. To detect Msn2 constructs, we incubated at 4°C overnight with 1:1000 mouse anti-RFP antibody (Chromotek 6G6) and incubated at room temperature for 1 h with 1:20,000 goat anti-mouse HRP-conjugated secondary antibody (ab97023). Bands were quantified in ImageJ following recommended practices.[51,57]

Sm-FISH—Strains were grown to mid-log and stimulated with a 40 min 300 μm/cm^2 blue light dose delivered by a calibrated light plate apparatus.[58,59] Stimulated cells were fixed and hybridized using Quasar 570-labeled FISH probes targeting mCitrine mRNA,[60] which were designed using the Stellaris Probe Designer and are listed in Table S3. Hybridized samples were stained with DAPI and imaged using a Nikon TiE inverted microscope with a 60x oil immersion objective and Cy3 (545/25x, 605/70m) and DAPI (350/50x, 460/50m) filter cubes. Images were acquired as z-stacks (focal plane ±2 μm in 0.2 μm increments).

QUANTIFICATION AND STATISTICAL ANALYSIS

Image analysis for light sweep experiments—Each light sweep experiment produced 32.ND2 timelapse images with 65 frames and 3 channels per frame: iRFP, mScarlet, and mCitrine. Because the optoPlate was mounted on top of the optical 96 well plate, we did not acquire images with transmitted light such as phase contrast or DIC images from which to segment cells. Likewise, because the mCitrine and mScarlet signals varied substantially over the course of an experiment—mCitrine was induced and mScarlet moved in and out of the nucleus—we segmented the cells from the iRFP images of the nuclear marker. This was done using custom image processing code written in MATLAB. Images were loaded

using the Bio-Formats MATLAB toolbox,[61] a Laplacian-of-Gaussian filter was applied to the iRFP images for blob enhancement, and a region of interest (ROI) representing each nucleus was segmented from the resulting high-contrast images using MATLAB's circle finder. This process largely excluded cells whose nuclei were out of focus. The circles were then enlarged by a factor of two to define a region of interest representing each cell, while the cytoplasm was defined as the region within each cell but outside the nucleus. If highly overlapping cells were identified, the cell with the lower "metric" value from MATLAB's circle finder was removed.

Using the ROIs defined during segmentation, the nuclear, cytoplasmic, and cellular fluorescence of each cell was quantified as the median pixel value of these regions in the raw iRFP, mScarlet, and mCitrine images. The background fluorescence in each channel was measured as the mode pixel value outside all cell ROIs. The resulting single-cell measurements were labeled with strain and light program information from the plate map associated with each experiment, as well as time information extracted from the.ND2 metadata. Measurements associated with aberrant frames in each timelapse, for example, due to shutter timing mismatches or temporary loss of focus, were identified as outliers in a plot of median iRFP versus frame and removed. Fluorescence differences due to long-term fluctuations in the Intensilight lamp intensity were corrected based on weekly lamp irradiance measurements. Photobleach correction was applied to the mCitrine measurements, but not mScarlet as the dynamic Msn2 localization time courses were not amenable to this approach. The median background mScarlet and mCitrine level per experiment was subtracted from the single-cell mScarlet and mCitrine measurements, respectively. Msn2 nuclear localization was quantified as nuclear mScarlet divided by cytoplasmic mScarlet. Basal Msn2 localization, quantified as the median Msn2 localization before the 0 min time point, was subtracted from the single-cell Msn2 nuclear localization measurements. The Msn2 localization measurements were then normalized to the maximum observed level of nuclear localization. Scripts for segmenting and measuring were deposited online (see key resources table).

The Msn2 localization and mCitrine induction time courses for each combination of Msn2-CLASP mutant and reporter were captured for three biological replicates across three separate experiments. As a result, the precise time at which each frame was captured varied by experiment. This was exacerbated in cases where refocusing was needed and led to issues when averaging fluorescence measurements across the three experiments, especially when a frame for one of the replicates was dropped. To account for these issues, the population level Msn2-CLASP localization and mCitrine induction time courses per condition were calculated by 1) taking the median localization or fluorescence measurement of all cells per frame, 2) assigning these values to bins representing 2.5 min segments of time, 3) filling in any missing values by linear interpolation. The mCitrine measurements for each replicate were smoothed using a 5-point moving average filter. Because Msn2(A)*-CLASP, Msn2*-CLASP, and Msn2(T)*-CLASP localize similarly in response to light, the AUC of Msn2 localization per condition was calculated from the mean localization of all three Msn2 mutants across all experiments. Measurements were plotted using the Gramm data visualization toolbox.[50] Measurements and scripts for generating plots were deposited online (see key resources table).

Flow cytometry quantification—The flow cytometry measurements were processed and analyzed using custom MATLAB tools. Measurements were imported from FCS files and automatically labeled from a plate map, an Excel spreadsheet file containing the strain and condition information for each well of the 384 well plate. The measurements were gated to remove debris and doublets and the median fluorescence intensity (MFI) was calculated for mScarlet and mCitrine per well. Measurement were plotted using the Gramm data visualization toolbox.[50] Scripts for processing and plotting flow cytometry measurements were deposited online (see key resources table).

FISH quantification—To quantify probe fluorescence from microscopy images, z-stacks were collapsed to a single maximum intensity projection image and the average Quasar 570 signal per cell was calculated from manually drawn regions of interest.

Statistical analysis—All statistical tests were performed in MATLAB. The KS test of Figure 2D was performed using the *kstest2* function. The two-way ANOVA test of Figure 5C was performed using the function *anovanFromSumStat* (see key resources table). The one-way ANOVA tests of Figures S4D and S4E were performed using the *anova1* function. Further details of statistical tests are provided in figure legends.

Supplementary Material

Refer to Web version on PubMed Central for supplementary material.

ACKNOWLEDGMENTS

We thank Susan Chen, Lindsey Osimiri, and Hana El-Samad for providing us with CLASP; Amit Nimunkar and Edvard Grødem for building and modifying our optoPlates; and Renee Szakaly for performing western blots. This work was supported by National Institutes of Health grant R35GM128873 and National Science Foundation grant 2045493 (awarded to M.N.M). Flow cytometry was enabled by the University of Wisconsin Carbone Cancer Center Support Grant P30 CA014520. M.N.M., PhD, holds a Career Award at the Scientific Interface from the Burroughs Wellcome Fund. K.S. was supported by an NHGRI Training grant 5T32HG002760 to the Genomic Sciences Training Program at the University of Wisconsin-Madison.

REFERENCES

1. Csete M, and Doyle J (2004). Bow ties, metabolism and disease. Trends Biotechnol. 22, 446–450. 10.1016/j.tibtech.2004.07.007. [PubMed: 15331224]
2. Chen SY, Osimiri LC, Chevalier M, Bugaj LJ, Nguyen TH, Green-stein RA, Ng AH, Stewart-Ornstein J, Neves LT, and El-Samad H (2020). Optogenetic control reveals differential promoter interpretation of transcription factor nuclear translocation dynamics. Cell Syst. 11, 336–353.e24. 10.1016/j.cels.2020.08.009. [PubMed: 32898473]
3. Cai L, Dalal CK, and Elowitz MB (2008). Frequency-modulated nuclear localization bursts coordinate gene regulation. Nature 455, 485–490. 10.1038/nature07292. [PubMed: 18818649]
4. Dalal CK, Cai L, Lin Y, Rahbar K, and Elowitz MB (2014). Pulsatile dynamics in the yeast proteome. Curr. Biol. 24, 2189–2194. 10.1016/j.cub.2014.07.076. [PubMed: 25220054]
5. Tay S, Hughey JJ, Lee TK, Lipniacki T, Quake SR, and Covert MW (2010). Single-cell NF-κB dynamics reveal digital activation and analogue information processing. Nature 466, 267–271. 10.1038/nature09145. [PubMed: 20581820]
6. Yissachar N, Sharar Fischler T, Cohen AA, Reich-zeliger S, Russ D, Shifrut E, Porat Z, and Friedman N (2013). Short article dynamic response diversity of NFAT isoforms in individual living cells. Mol. Cell 49, 322–330. 10.1016/j.molcel.2012.11.003. [PubMed: 23219532]

7. Batchelor E, Loewer A, Mock C, and Lahav G (2011). Stimulus-dependent dynamics of p53 in single cells. Mol. Syst. Biol. 7, 488. 10.1038/msb.2011.20. [PubMed: 21556066]
8. Chen L.f., Mu Y, and Greene WC (2002). Acetylation of RelA at discrete sites regulates distinct nuclear functions of NF-κB. EMBO J. 21, 6539–6548. 10.1093/emboj/cdf660. [PubMed: 12456660]
9. Kiernan R, Brès V, Ng RWM, Coudart MP, El Messaoudi S, Sardet C, Jin DY, Emiliani S, and Benkirane M (2003). Post-activation turn-off of NF-κB-dependent transcription is regulated by acetylation of p65. J. Biol. Chem. 278, 2758–2766. 10.1074/jbc.M209572200. [PubMed: 12419806]
10. Crawley CD, Raleigh DR, Kang S, Voce DJ, Schmitt AM, Weich-selbaum RR, and Yamini B (2013). DNA damage-induced cytotoxicity is mediated by the cooperative interaction of phospho-NF-κB p50 and a single nucleotide in the kb-site. Nucleic Acids Res. 41, 764–774. 10.1093/nar/gks1120. [PubMed: 23180782]
11. Ea CK, and Baltimore D (2009). Regulation of NF-κB activity through lysine monomethylation of p65. Proc. Natl. Acad. Sci. USA 106, 18972–18977. 10.1073/pnas.0910439106. [PubMed: 19864627]
12. Werner SL, Barken D, and Hoffmann A (2005). Stimulus specificity of gene expression programs determined by temporal control of IKK activity. Science 309, 1857–1861. 10.1126/science.1113319. [PubMed: 16166517]
13. Purvis JE, Karhohs KW, Mock C, Batchelor E, Loewer A, and Lahav G (2012). p53 dynamics control cell fate. Science 336, 1440–1444. 10.1126/science.1218351. [PubMed: 22700930]
14. Gu W, and Roeder RG (1997). Activation of p53 sequence-specific DNA binding by acetylation of the p53 C-terminal domain. Cell 90, 595–606. 10.1016/S0092-8674(00)80521-8. [PubMed: 9288740]
15. Sykes SM, Mellert HS, Holbert MA, Li K, Marmorstein R, Lane WS, and McMahon SB (2006). Acetylation of the p53 DNA-binding domain regulates apoptosis induction. Mol. Cell 24, 841–851. 10.1016/j.molcel.2006.11.026. [PubMed: 17189187]
16. He F, Borcherds W, Song T, Wei X, Das M, Chen L, and Daughdrill GW (2019). Interaction between p53 N terminus and core domain regulates specific and nonspecific DNA binding. Biochemistry 116, 8859–8868. 10.1073/pnas.1903077116.
17. Vonderach M, Byrne DP, Barran PE, Eyers PA, and Eyers CE (2019). DNA binding and phosphorylation regulate the core structure of the NF-κB p50 transcription factor. J. Am. Soc. Mass Spectrom. 30, 128–138. 10.1007/s13361-018-1984-0. [PubMed: 29873020]
18. Gasch AP, Spellman PT, Kao CM, Carmel-Harel O, Eisen MB,Storz G, Botstein D, and Brown PO (2000). Genomic expression programs in the response of yeast cells to environmental changes. Mol. Biol. Cell 11, 4241–4257. 10.1091/mbc.11.12.4241. [PubMed: 11102521]
19. Petrenko N, Chereji RV, McClean MN, Morozov AV, and Broach JR (2013). Noise and interlocking signaling pathways promote distinct transcription factor dynamics in response to different stresses. Mol. Biol. Cell 24, 2045–2057. 10.1091/mbc.E12-12-0870. [PubMed: 23615444]
20. Görner W, Durchschlag E, Martinez-Pastor MT, Estruch F, Ammerer G, Hamilton B, Ruis H, and Schüller C (1998). Nuclear localization of the C2H2 zinc finger protein Msn2p is regulated by stress and protein kinase A activity. Genes Dev. 12, 586–597. 10.1101/gad.12.4.586. [PubMed: 9472026]
21. Hao N, and O'Shea EK (2011). Signal-dependent dynamics of transcription factor translocation controls gene expression. Nat. Struct. Mol. Biol. 19, 31–39. 10.1038/nsmb.2192. [PubMed: 22179789]
22. Hansen AS, and O'Shea EK (2013). Promoter decoding of transcription factor dynamics involves a trade-off between noise and control of gene expression. Mol. Syst. Biol. 9, 704. 10.1038/msb.2013.56. [PubMed: 24189399]
23. Hansen AS, and O'Shea EK (2015). Cis determinants of promoter threshold and activation timescale. Cell Rep. 12, 1226–1233. 10.1016/j.celrep.2015.07.035. [PubMed: 26279577]
24. Bodvard K, Peeters K, Roger F, Romanov N, Igbaria A, Welkenhuysen N, Palais G, Reiter W, Toledano MB, Käll M, et al. (2017). Light-sensing via hydrogen peroxide and a peroxiredoxin. Nat. Commun. 8, 14791. 10.1038/ncomms14791. [PubMed: 28337980]

25. Hao N, Budnik B. a, Gunawardena J, and O'Shea EK. (2013). Tunable signal processing through modular control of transcription factor translocation. Science 339, 460–464. 10.1126/science.1227299. [PubMed: 23349292]
26. Durchschlag E, Reiter W, Ammerer G, and Schuller C (2004). Nuclear€ localization destabilizes the stress-regulated transcription factor Msn2. J. Biol. Chem. 279, 55425–55432. 10.1074/jbc.M407264200. [PubMed: 15502160]
27. Lallet S, Garreau H, Poisier C, Boy-Marcotte E, and Jacquet M (2004). Heat shock-induced degradation of Msn2p, a Saccharomyces cerevisiae transcription factor, occurs in the nucleus. Mol. Genet. Genomics. 272, 353–362. 10.1007/s00438-004-1063-z. [PubMed: 15375696]
28. Sadeh A, Movshovich N, Volokh M, Gheber L, Aharoni A, and Boone C (2011). Fine-tuning of the Msn2/4 – mediated yeast stress responses as revealed by systematic deletion of Msn2/4 partners. Mol. Biol. Cell 22, 3127–3138. 10.1091/mbc.E10-12-1007. [PubMed: 21757539]
29. Benman W, Berlew EE, Deng H, Parker C, Kuznetsov IA, Lim B, Siekmann AF, Chow BY, and Bugaj LJ (2022). Temperature-responsive optogenetic probes of cell signaling. Nat. Chem. Biol. 18, 152–160. 10.1038/s41589-021-00917-0. [PubMed: 34937907]
30. Stewart-Ornstein J, Nelson C, Derisi J, Weissman JS, and El-Samad H (2013). Msn2 coordinates a stoichiometric gene expression program. Curr. Biol. 23, 2336–2345. 10.1016/j.cub.2013.09.043. [PubMed: 24210615]
31. Pfanzagl V, Görner W, Radolf M, Parich A, Schuhmacher R, Strauss J, Reiter W, and Schüller C (2018). A constitutive active allele of the transcription factor Msn2 mimicking low PKA activity dictates metabolic remodeling in yeast. Mol. Biol. Cell 29, 2848–2862. 10.1091/mbc.E18-06-0389. [PubMed: 30256697]
32. Reiter W, Klopf E, De Wever V, Anrather D, Petryshyn A, Roetzer A, Niederacher G, Roitinger E, Dohnal I, Görner W, et al. (2013). Yeast protein phosphatase 2A-Cdc55 regulates the transcriptional response to hyperosmolarity stress by regulating Msn2 and Msn4 chromatin recruitment. Mol. Cell Biol. 33, 1057–1072. 10.1128/mcb.00834-12. [PubMed: 23275436]
33. Chang YW, Howard SC, and Herman PK (2004). The Ras/PKA signaling pathway directly targets the Srb9 protein, a component of the general RNA polymerase II transcription apparatus. Mol. Cell 15, 107–116. 10.1016/j.molcel.2004.05.021. [PubMed: 15225552]
34. Pincus D, Aranda-Díaz A, Zuleta IA, Walter P, and El-samad H (2014). Delayed Ras/PKA signaling augments the unfolded protein response. Proc. Natl. Acad. Sci. USA 111, 14800–14805. 10.1073/pnas.1409588111. [PubMed: 25275008]
35. Gutin J, Sadeh A, Rahat A, Aharoni A, and Friedman N (2015). Condition-specific genetic interaction maps reveal crosstalk between the cAMP/PKA and the HOG MAPK pathways in the activation of the general stress response. Mol. Syst. Biol. 11, 829. 10.15252/msb.20156451. [PubMed: 26446933]
36. Lee P, Cho B-R, Joo H-S, and Hahn J-S (2008). Yeast Yak1 kinase, a bridge between PKA and stress-responsive transcription factors, Hsf1 and Msn2/Msn4. Mol. Microbiol. 70, 882–895. 10.1111/j.1365-2958.2008.06450.x. [PubMed: 18793336]
37. Aditham AK, Markin CJ, Mokhtari DA, DelRosso N, and Fordyce PM (2021). High-throughput affinity measurements of transcription factor and DNA mutations reveal affinity and specificity determinants. Cell Syst. 12, 112–127.e11. 10.1016/j.cels.2020.11.012. [PubMed: 33340452]
38. Crocker J, Preger-Ben Noon E, and Stern DL (2016). The Soft Touch: Low-Affinity Transcription Factor Binding Sites in Development and Evolution, 1st ed (Elsevier Inc.). 10.1016/bs.ctdb.2015.11.018.
39. Hansen AS, and O'Shea EK (2015). Limits on information transduction through amplitude and frequency regulation of transcription factor activity. Elife 4, e06559. 10.7554/eLife.06559. [PubMed: 25985085]
40. Lin Y, Sohn CH, Dalal CK, Cai L, and Elowitz MB (2015). Combinatorial gene regulation by modulation of relative pulse timing. Nature 527, 54–58. 10.1038/nature15710. [PubMed: 26466562]
41. Benzinger D, Ovinnikov S, and Khammash M (2022). Synthetic gene networks recapitulate dynamic signal decoding and differential gene expression. Cell Syst. 13, 353–364.e6. 10.1016/j.cels.2022.02.004. [PubMed: 35298924]

42. Gasch AP, Yu FB, Hose J, Escalante LE, Place M, Bacher R, Kanbar J, Ciobanu D, Sandor L, Grigoriev IV, et al. (2017). Single-cell RNA sequencing reveals intrinsic and extrinsic regulatory heterogeneity in yeast responding to stress. PLoS Biol. 15, e2004050. [PubMed: 29240790]
43. Lam FH, Steger DJ, and O'Shea EK (2008). Chromatin decouples promoter threshold from dynamic range. Nature 453, 246–250. 10.1038/nature06867. [PubMed: 18418379]
44. Sharon E, Kalma Y, Sharp A, Raveh-Sadka T, Levo M, Zeevi D, Keren L, Yakhini Z, Weinberger A, and Segal E (2012). Inferring gene regulatory logic from high-throughput measurements of thousands of systematically designed promoters. Nat. Biotechnol. 30, 521–530. 10.1038/nbt.2205. [PubMed: 22609971]
45. Sen S, Cheng Z, Sheu KM, Chen YH, and Hoffmann A (2020). Gene regulatory strategies that decode the duration of NF-κB dynamics contribute to LPS- versus TNF-specific gene expression. Cell Syst. 10, 169–182.e5. 10.1016/j.cels.2019.12.004. [PubMed: 31972132]
46. Cheng QJ, Ohta S, Sheu KM, Spreafico R, Adelaja A, Taylor B, and Hoffmann A (2021). NF-κB dynamics determine the stimulus specificity of epigenomic reprogramming in macrophages. Science 372, 1349–1353. 10.1126/science.abc0269. [PubMed: 34140389]
47. Lickwar CR, Mueller F, Hanlon SE, McNally JG, and Lieb JD (2012). Genome-wide protein-DNA binding dynamics suggest a molecular clutch for transcription factor function. Nature 484, 251–255. 10.1038/nature10985. [PubMed: 22498630]
48. Larson DR, Fritzsch C, Sun L, Meng X, Lawrence DS, and Singer RH (2013). Direct observation of frequency modulated transcription in single cells using light activation. Elife 2, e00750. 10.7554/eLife.00750. [PubMed: 24069527]
49. Tutucci E, Vera M, Biswas J, Garcia J, Parker R, and Singer RH (2018). An improved MS2 system for accurate reporting of the mRNA life cycle. Nat. Methods 15, 81–89. 10.1038/nmeth.4502. [PubMed: 29131164]
50. Morel P (2018). Gramm: grammar of graphics plotting in Matlab. J. Open Source Softw. 3, 568. 10.21105/joss.00568.
51. Schneider CA, Rasband WS, and Eliceiri KW (2012). NIH Image to ImageJ: 25 years of image analysis. Nat. Methods 9, 671–675. 10.1038/nmeth.2089. [PubMed: 22930834]
52. Bugaj LJ, and Lim WA (2019). High-throughput multicolor optogenetics in microwell plates. Nat. Protoc. 14, 2205–2228. 10.1038/s41596-019-0178-y. [PubMed: 31235951]
53. Grødem EO, Sweeney K, and McClean MN (2020). Automated calibration of optoPlate LEDs to reduce light dose variation in optogenetic experiments. Biotechniques 69, 313–316. 10.2144/BTN-2020-0077. [PubMed: 32722938]
54. Gietz RD, and Schiestl RH (2007). High-efficiency yeast transformation using the LiAc/SS carrier DNA/PEG method. Nat. Protoc. 2, 31–34. 10.1038/nprot.2007.13. [PubMed: 17401334]
55. Lee ME, Deloache WC, Cervantes B, and Dueber JE (2015). A Highly Characterized Yeast Toolkit for Modular, Multipart Assembly. 10.1021/sb500366v.
56. Sheff MA, and Thorn KS (2004). Optimized cassettes for fluorescent protein tagging in Saccharomyces cerevisiae. Yeast 21, 661–670. 10.1002/yea.1130. [PubMed: 15197731]
57. Gassmann M, Grenacher B, Rohde B, and Vogel J (2009). Quantifying Western blots: pitfalls of densitometry. Electrophoresis 30, 1845–1855. 10.1002/elps.200800720. [PubMed: 19517440]
58. Sweeney K, Moreno Morales N, Burmeister Z, Nimunkar AJ, and McClean MN (2019). Easy calibration of the light plate apparatus for optogenetic experiments. MethodsX 6, 1480–1488. 10.1016/j.mex.2019.06.008. [PubMed: 31293905]
59. Gerhardt KP, Olson EJ, Castillo-Hair SM, Hartsough LA, Landry BP, Ekness F, Yokoo R, Gomez EJ, Ramakrishnan P, Suh J, et al. (2016). An open-hardware platform for optogenetics and photobiology. Sci. Rep. 6, 35363. 10.1038/srep35363. [PubMed: 27805047]
60. McIsaac RS, Silverman SJ, Parsons L, Xu P, Briehof R, McClean MN, and Botstein D (2013). Visualization and analysis of mRNA molecules using fluorescence in situ hybridization in Saccharomyces cerevisiae. J. Vis. Exp. 1, e50382. 10.3791/50382.
61. Linkert M, Rueden CT, Allan C, Burel JM, Moore W, Patterson A, Loranger B, Moore J, Neves C, MacDonald D, et al. (2010). Metadata matters: access to image data in the real world. J. Cell Biol. 189, 777–782. 10.1083/jcb.201004104. [PubMed: 20513764]

Highlights

- Gene promoters decode light-controlled transcription factor (TF) dynamics
- Effect of changing TF affinity for DNA on decoding is highly promoter dependent
- Relative response to pulsed versus continuous doses of TF set primarily by promoter
- Concerted regulation of TF affinity and localization improves control of expression

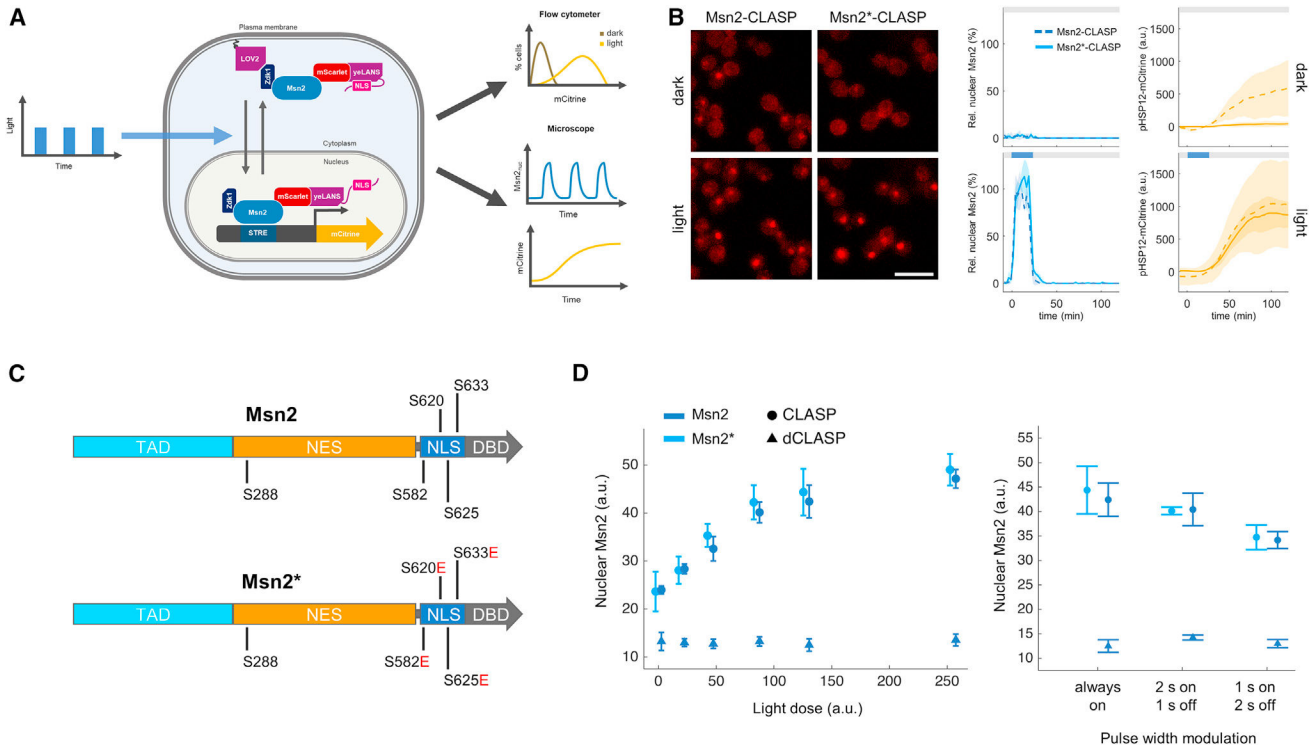

Figure 1. Optogenetic control of Msn2 localization using CLASP

(A) A schematic of the Msn2-CLASP system and experiments in which time-varying light doses drove corresponding patterns of Msn2-CLASP nuclear localization and gene expression.

(B) (Left) Micrographs showing Msn2-CLASP and Msn2*-CLASP localizing to the nucleus following 255 a.u. blue light (scale bar, 10 μm). Light-induced nuclear localization (middle) and reporter gene induction (right) by Msn2-CLASP (dashed lines) and Msn2*-CLASP (solid lines) following a 10 min pulse of 128 a.u. blue light (depicted by blue boxes). Data represent mean ± standard deviation (SD) for three biological replicates, each with ≥47 cells.

(C) Schematic showing Msn2 functional domains—the transactivation domain (TAD), nuclear export signal (NES), nuclear localization signal (NLS), and zinc finger DNA-binding domain (DBD)—and residues mutated for improved optogenetic control.

(D) (Left) Absolute nuclear Msn2-CLASP, Msn2*-CLASP, and Msn2-dCLASP following 15 min doses of blue light with intensities ranging from 0 to 255 a.u. (i.e., irradiances of 0–405 μW/cm^2, see Figure S1C). (Right) Nuclear Msn2-CLASP and Msn2*-CLASP in response to 128 a.u. blue light with varying degrees of pulse width modulation (PWM). Data represent mean ± SD of three biological replicates, each with ≥43 cells. Measurements were acquired by fluorescence microscopy.

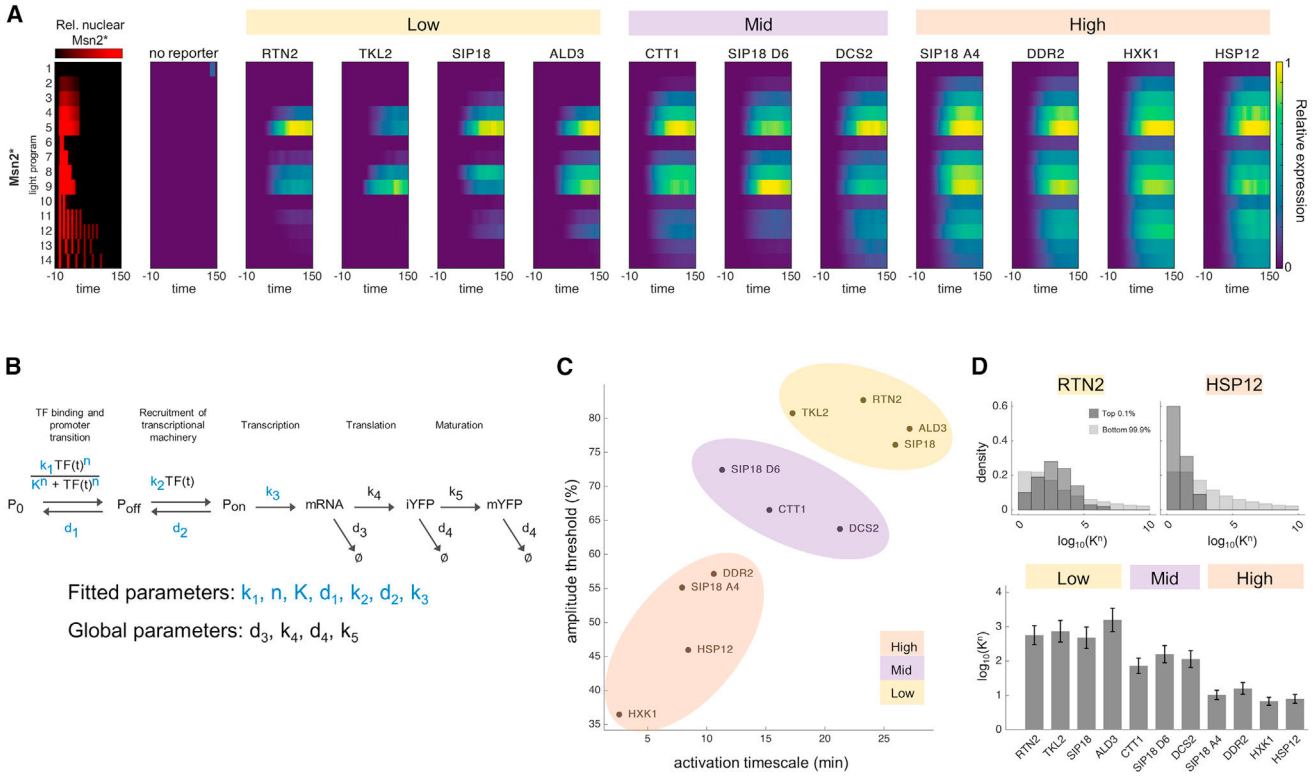

Figure 2. Light-sweep experiments and model-based characterization of Msn2 target genes

(A) Light-sweep experiments probe how promoters decode the nuclear localization dynamics of Msn2*. Each row represents a light program that drove Msn2 localization (left) and reporter expression (right). Msn2* localization measurements were pooled over many experiments and represent thousands of cells per condition. Expression measurements were normalized to maximum expression per reporter across all conditions and represent mean of ~100–600 cells per condition from three biological replicates. For comparison, figure layout is adapted from Hansen and O'Shea.[22] See also Figure S2A.

(B) Schematic of gene expression model. See STAR Methods for corresponding system of ordinary differential equations (ODEs) and Figure S2A for plots of fits.

(C) Categorization of promoters based on how they decoded single pulses of nuclear Msn2*.

(D) (Top) Predicted values of K^n obtained from the gene expression model for top 0.1% and bottom 99.9% of parameter sets; two-sample Kolmogorov-Smirnov (KS) tests showed differences between these distributions ($p = 0.0015$ for *RTN2* and $p < 10^{-24}$ for *HSP12*). (Bottom) Predicted affinity of each promoter for Msn2*. Data represent mean ±95% confidence interval (CI) for top 0.1% of parameter sets per promoter.

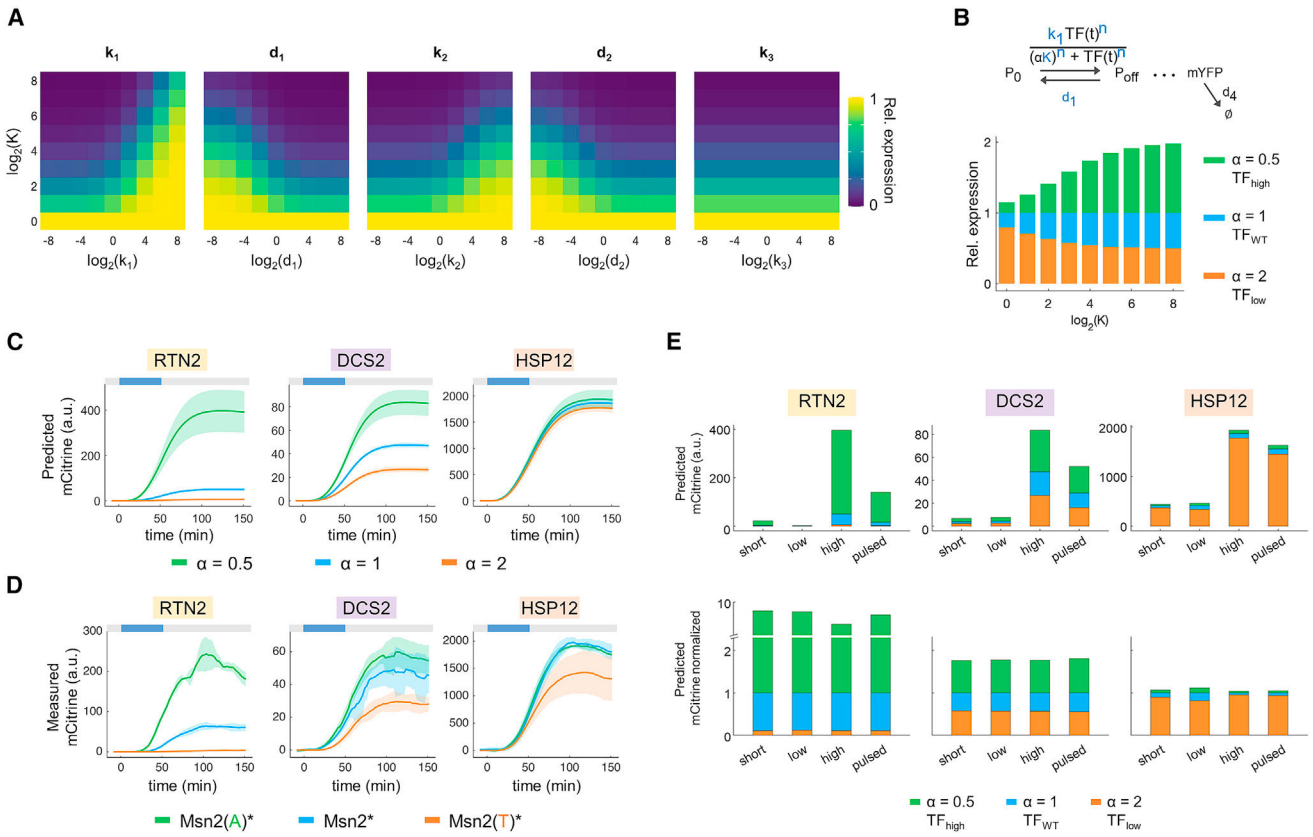

Figure 3. Simulations demonstrate that changes in TF affinity for DNA have a strong effect on low-sensitivity promoters and a weak effect on high-sensitivity promoters

(A) Simulated maximum expression of hypothetical promoters for a 50 min 100% amplitude pulse of nuclear TF. Each kinetic parameter (k_1, d_1, k_2, d_2, and k_3) was varied, while other kinetic parameters were fixed to one (with n = 1). Simulations were repeated for varying values of K. Expression was normalized to case where K = 1 (bottom square of each column).

(B) (Top) Modified gene expression model in which changes in Msn2 affinity for DNA are modeled by scaling K by α. Omitted model steps are shown in Figure 2B. (Bottom) Maximum predicted expression of hypothetical promoters with a range of baseline affinities (K) for a 50 min 100% amplitude pulse of TF (other kinetic parameters were fixed to one). To model the additional effect of a 2-fold increase or decrease in TF binding affinity, simulations were repeated while scaling K by α = 0.5 or 2, respectively. Expression of each hypothetical promoter was normalized to case where α = 1, which represents the affinity between the promoter and the wild-type (WT) TF.

(C) Predicted reporter expression following a 50 min 100% amplitude pulse of nuclear Msn2* (shown in blue, assumes α = 1). To model the additional effect of a 2-fold increase or decrease in the affinity of Msn2 for DNA, simulations were repeated while scaling K by α = 0.5 or 2, respectively (as depicted in B, top). Data represent mean ±95% CI of predicted expression for top 10 parameter sets for each reporter.

(D) Measured reporter expression following a 50 min 100% amplitude pulse of nuclear localization for Msn2* and high- and low-affinity mutants Msn2(A)* andMsn2(T)*. Data represent mean ± SD for three biological replicates.

(E) Maximum predicted reporter expression for a 10 min 100% amplitude pulse of nuclear Msn2* (short), a 50 min 25% amplitude pulse (low), a 50 min 100%amplitude pulse (high; time courses shown in C), and six 5 min pulses with 100% amplitude and 5 min interpulse durations (pulsed). As above, simulations were repeated while scaling α to capture changes in Msn2 affinity. Data represent mean of maximum expression predicted for top 10 parameter sets per reporter. (Bottom) Predicted maximum reporter expression at each condition normalized to predicted expression for Msn2* (where $\alpha = 1$).

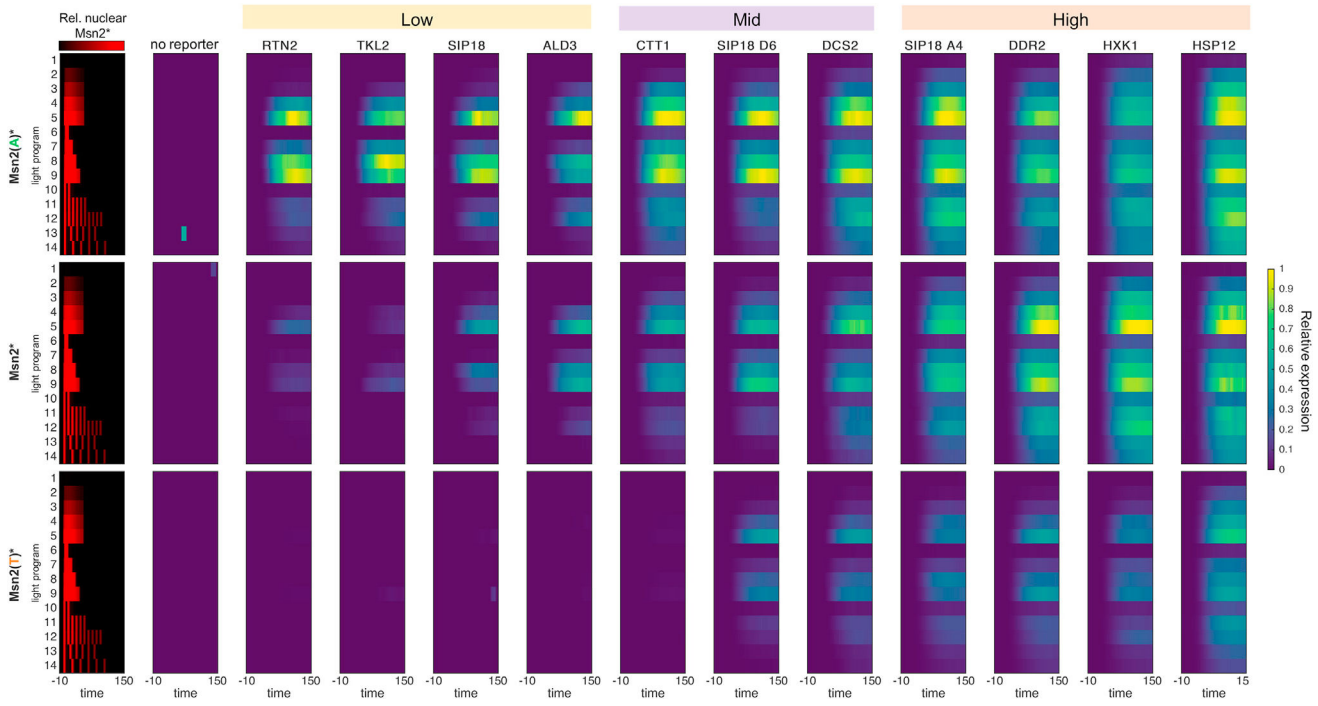

Figure 4. Light-sweep experiments with Msn2 DBD mutants reveal the differential effects of changing TF affinity on the signal decoding behaviors of promoters

Each row corresponds to a light program, which drove Msn2 localization (left) and subsequent gene expression (right). Msn2 localization measurements were pooled over many experiments and represent thousands of cells per condition. Gene expression measurements were normalized to the maximum expression level per reporter across all conditions and Msn2 DBD mutants and represent mean of ~100–600 cells from three biological replicates. See also Figure S2A.

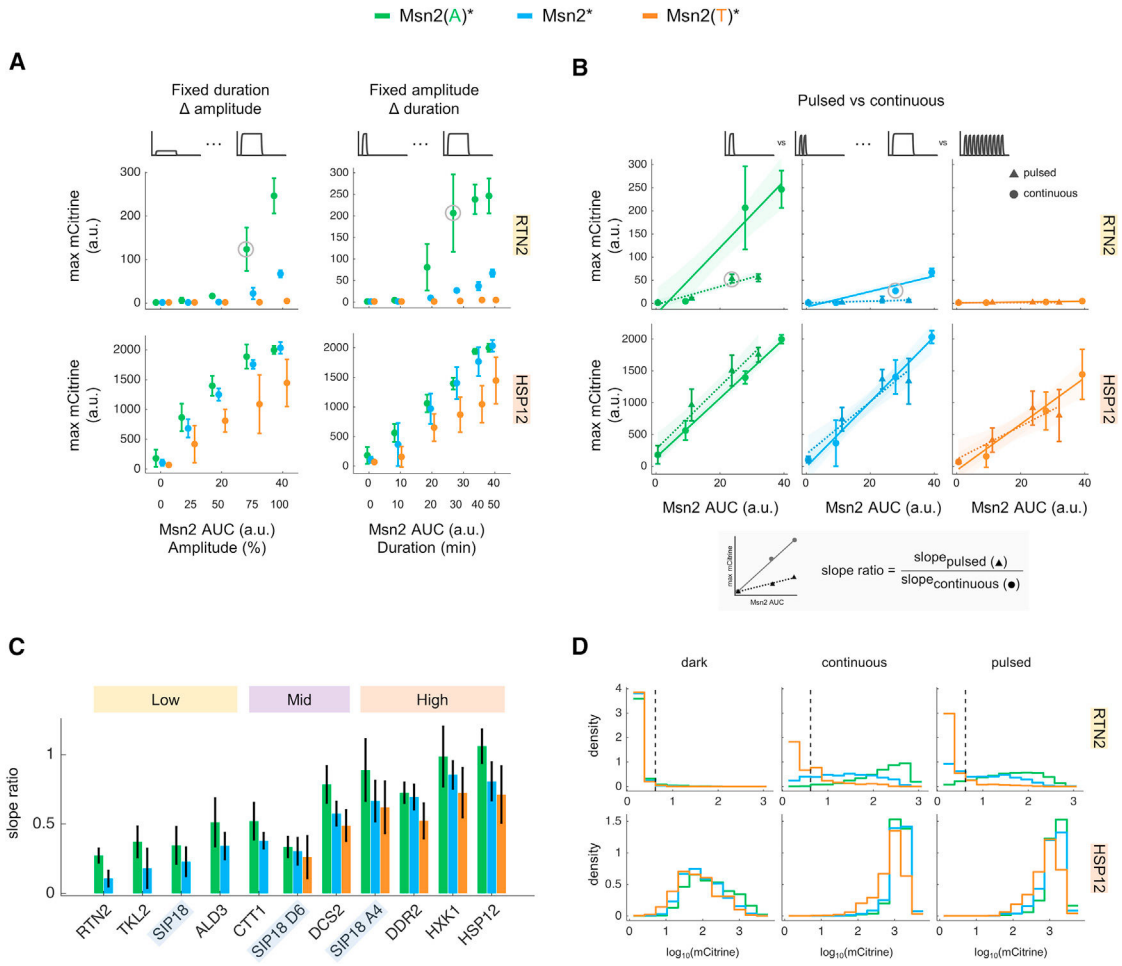

Figure 5. Analyzing the decoding behavior of high- and low-sensitivity promoters

(A) Maximum reporter expression following 50 min pulses of each Msn2 DBD mutant with amplitudes ranging from 0% to 100% (left) or 100% amplitude pulses with durations varying from 0 to 50 min (right). Data represent mean ± SD for three biological replicates. Gray circles denote conditions referenced in the main text.

(B) Maximum reporter expression for pulsatile versus continuous doses of each Msn2 mutant. Circles represent maximum expression for 100% amplitude continuous pulses of nuclear Msn2 with durations of 0, 10, 30, and 50 min. Triangles represent maximum expression following 0, 2, 6, or 10 5 min pulses of nuclear Msn2 with 100% amplitude and 5 min interpulse durations. Data represent mean ± SD for three biological replicates. Solid and dashed lines show best fit lines for continuous and pulses conditions, respectively; shaded regions show 95% CI of best fit lines. Gray circles denote conditions referenced in main text.

(C) Reporter slope ratios. Data represent mean ± SD of slope ratio per promoter and Msn2 DBD mutant. A two-way ANOVA test revealed significant differences in slope ratio between promoters and Msn2 DBD mutants, though differences between promoters were generally larger in magnitude.

(D) Reporter expression for cells exposed to no light (dark), a 30 min 100% amplitude pulse of nuclear Msn2 (continuous), or six 5 min 100% amplitude pulses with 5 min interpulse

durations (pulsed). Histograms represent single-cell fluorescence measurements for three biological replicates between 115 and 125 min. Dashed line represents the threshold above which *RTN2* was considered active (calculated as 99th percentile *RTN2* level in dark).

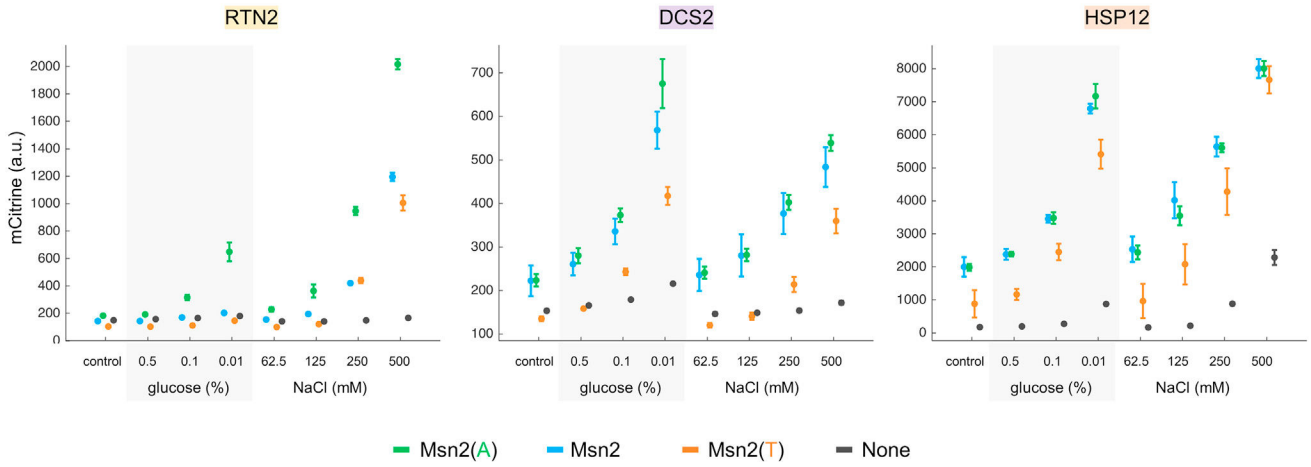

Figure 6. Changing Msn2 affinity can alter the ability of promoters to discriminate between stresses

Fluorescent reporter expression following 2 h of glucose starvation or hyperosmotic shock. All Msn2 mutants were expressed in the dCLASP system and had no mutations outside the DBD. Data represent mean ± SD for at least three biological replicates. See also Figure S6A.

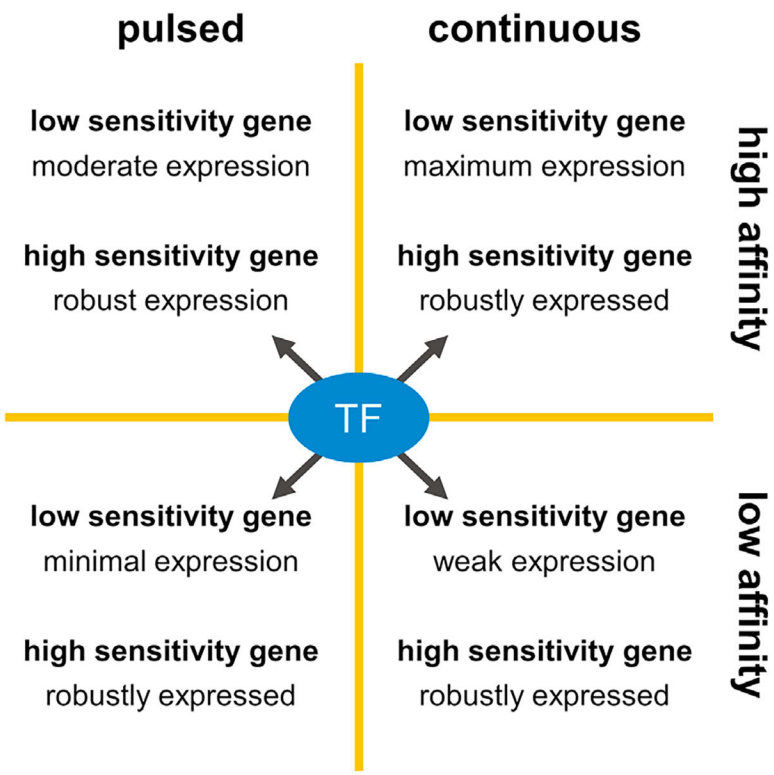

Figure 7. Concerted regulation of TF affinity and dynamics may facilitate improved control of gene expression

A TF that can transition between high- and low-affinity binding modes and continuous and pulsatile nuclear localization patterns could tune the expression of low-sensitivity genes while maintaining robust activation of high-sensitivity genes. Schematic is based on single-cell expression measurements of Figure 4C, where a pulsed dose of Msn2(T)* mutant minimally activated the low-sensitivity gene *RTN2*, while a continuous dose of Msn2(T)* weakly activated *RTN2*. In contrast, a pulsed dose of Msn2(A)* mutant moderately activated *RTN2* and a continuous dose maximized *RTN2* activation. Meanwhile, a dose of either Msn2(T)* or Msn2(A)* could robustly activate the high-sensitivity gene *HSP12*.